

A correlation analysis of flux ratios and the Doppler factor for EGRET AGN sources

L.H. Huang, D.R. Jiang, Xinwu Cao

Shanghai Observatory, Chinese Academy of Sciences, 80 Nandan Road, Shanghai, 200030, P.R. China

Abstract. We present a correlation analysis between the flux ratio of high-energy γ -ray emission to synchrotron emission and the Doppler factor for a sample of EGRET AGNs. The result favors a model that attributes the EGRET emission of AGNs to inverse-Compton scattering on photons external to the jet.

Key words: galaxies: kinematics and dynamics - galaxies: nuclei, jets.

1. Introduction

Since its launch in April 1991, the experiments on board of the Compton Gamma Ray Observatory have detected many active galactic nuclei (AGNs) at photon energies $> 100\text{MeV}$. 42 AGNs have recently been identified as EGRET sources with high confidence (Mattox 1997). A common characteristic of these sources is that they all are radio-loud, flat spectrum radio sources. Many of them are seen as superluminal radio sources as well ($> 25\%$). All these AGNs belong to the blazar category (containing BL Lac objects, highly polarized ($> 3\%$) quasars (HPQ), and optically violently variable (OVV) quasars), where relativistic beaming is thought to play an important role in the γ -ray emission. In fact, strong evidence for relativistic motion of the emitting plasma has been provided by the observation of superluminal expansion of radio knots to the radio core in numerous blazars (Vermeulen & Cohen 1994).

Observationally, blazar energy spectra appear to be contained of at least two components: a low-energy component with luminosity (νL_ν) peaking in the IR-UV range, and a high-energy component with luminosity (νL_ν) strongly dominated by hard γ -rays, at least in those sources detected by EGRET. The division of spectra into two components is reflected by the deep drop

of the low-energy component toward the far-UV band (Impey & Neugebauer 1988; Brown et al. 1989a, 1989b), and the rise of νL_ν toward higher energies in the X-ray band, observed clearly in most OVV quasars (Worrall & Wilkes 1990) and most radio selected BL Lac objects (Sambruna et al. 1996). The simplest models addressing the double-component nature of blazar spectra are those in which the low-energy component is produced by synchrotron radiation and the high-energy component is produced by the inverse-Compton process. A variety of models have recently been proposed to explain the origin of the γ -ray emission, including synchrotron-self-Compton (SSC) radiation (Jones et al. 1974; Marscher 1980; Königl 1981; Marscher & Gear 1985; Ghisellini & Maraschi 1989; Maraschi et al. 1992) and inverse-Compton scattering on photons produced by the accretion disc (Melia & Königl 1989; Dermer et al. 1992; Dermer & Schlickeiser 1993), the broad-line region (e.g. Sikora et al. 1994) or the dusty torus (Wagner et al. 1995a). In addition to these models, there are also other models devoted to understand the γ -ray emission mechanism of AGNs such as: diffusive shock acceleration in electron-proton jets producing high-energy emission through photomeson production and the subsequent cascade of secondary particles (Mannheim & Biermann 1992; Mannheim 1993a, 1993b); synchrotron radiation in regions of high magnetic fields (Ghisellini 1993); and radiation from secondary electrons resulting from decays of ultrarelativistic neutrons emitted by the central engine (e. g. Mastichiadis & Protheroe 1990).

Considering the strong association of identified EGRET AGN sources with the blazar class, the fact that nearly 25% of the EGRET AGN sources are superluminal, and the success of jet models in explaining the non-thermal radiation from blazars, we will focus our discussion on γ -ray emission models associated with jets. In fact, lately it has been established for the blazars 0528+134 (Pohl et al. 1995), 3C279 (Wehrle et al. 1996) and 1633+382 (Barthel et al. 1995) that enhanced levels of activity in the optical and γ -ray bands are associated with the emergence of new jet components. In several models

that have been proposed, the γ -ray emission originates in a jet as a product of inverse-Compton scattering of relativistic electrons and seed photons produced externally to the jet (Dermer et al. 1992; Sikora et al. 1994; Wagner et al. 1995a). The importance of the process depends on the dominance of the externally produced radiation energy density (as seen in the comoving frame of the jet) with respect to magnetic energy density and the energy density of the radiation produced internally. If the seed photons are produced externally to the jet, then one can predict a correlation between the Doppler factor δ and the ratio of the γ -ray flux to the synchrotron radiation flux, $(\nu F_\nu)_\gamma / (\nu F_\nu)_{syn}$, as was shown by Eq. (27) in Dermer et al. (1997):

$$\rho = \frac{(\nu F_\nu)_\gamma}{(\nu F_\nu)_{syn}} \approx k \delta^{1+\alpha} \quad (1)$$

where $k = U_{iso}/U_b$ denotes the ratio of the energy density in the external target radiation field and the blob's magnetic field. The ratio of the SSC spectral power flux at energy ϵ_C to the synchrotron spectral power flux at energy ϵ_s is given by Eq. (28) in Dermer et al. (1997):

$$\rho = \frac{2}{3} (\sigma_T n_{eo} r_b) \left(\frac{\epsilon_s}{\epsilon_C} \right)^{\alpha-1} \ln \Sigma_C(\epsilon_C) \rho_{SSC/syn} \quad (2)$$

Where r_b is the radius of the blob, assumed to be spherical in the comoving frame, and n_{eo} is the number density of nonthermal electrons. Therefore, the flux ratio in the SSC model is independent of the Doppler factor. With the requirement that γ -rays do not interact with X-rays (assumed cospatial) through photon-photon collisions, Dondi & Ghisellini calculated the lower limit on the Doppler boosting factor δ of the γ -ray emission for a sample of EGRET sources and found that relativistic motion is required in all cases. They compared the derived δ with other beaming factors such as the ratio between the γ -ray flux density and the optical flux density, and found no obvious relation between the two different beaming factors.

The emission models mentioned above imply a variety of relations between the emissions in different wavelength bands that can be used to distinguish among them observationally. In this paper, we present a compilation of flux densities in different wavelength bands for 27 blazars which are considered to be EGRET sources with high confidence (Mattox et al. 1997) and the VLBI data of these sources if available. The data selection is described in Sect. 2. In Sect. 3 we calculate the ratios of the γ -ray flux density (here defined as νF_ν) to the optical flux density, the near-infrared (at $2.2 \mu\text{m}$) flux density, and the millimeter (90 GHz, 230 GHz) flux density. We derive the Doppler factor based on the synchrotron-self-Compton model (Ghisellini et al. 1993), and we investigate the correlation between the flux ratio and the Doppler factor by using a linear regression analysis. In Sect. 4, these correlation results are compared with theoretical results and their physical meaning is discussed.

2. Sample

Mattox et al. (1997) developed an analysis of EGRET radio source identification that quantitatively incorporates a lot of important information such as the size of the EGRET error region, the number density of potentially confusing radio sources, the radio spectral index and the a priori probability of detecting a radio source by EGRET. They provided a table of 42 blazars that were considered to be robust identifications of EGRET sources. In this paper, we will focus on a subset of these sources. They are listed in Table 1, whose columns are: (1) IAU name; (2) classification of the source (B=BL Lac object, HPQ=highly polarized quasar, LPQ=low polarized quasar, NP=no polarization measurement); (3) redshift; (4) γ -ray flux density above 100 MeV, F_γ , in units of $10^{-8} \text{ photon cm}^{-2} \text{ s}^{-1}$; (5) spectral index of the γ -ray energy spectrum; (6) reference for the γ -ray flux density and spectral index; (7) V-band optical flux density F_o in mJy; (8) reference for the optical flux density; (9) near infrared flux density F_{IR} (at $2.2 \mu\text{m}$) in mJy; (10) reference for the infrared flux density; (11) flux density at 90 GHz; (12) reference for the flux density at 90 GHz; (13) flux density at 230 GHz; (14) reference for the flux density at 230 GHz. Table 1 lists 27 blazars which have been identified with high confidence by Mattox et al (1997) and for which VLBI and X-ray observations (1 keV) are available. All sources in Table 2 are known to be variable, but only a few sources have been observed simultaneously at different wavelengths such as 3C273, 3C279. We therefore choose to list the highest flux densities for all sources from the literature, irrespective of the dates of the observations. The optical fluxes are mainly chosen from Dondi & Ghisellini (1995) who have chosen the maxima from the literature. The highest flux densities at 90 GHz and 230 GHz are mainly chosen from Steppe et al. (1988, 1992). The classifications mainly refer to Dondi & Ghisellini (1995) and Ghisellini et al. (1993). Table 2 lists the VLBI and X-ray observations; (1) IAU name; (2) redshift; (3) VLBI core size(θ_d) in mas; (4) core radio flux density (F_c) at frequency ν_s ; (5) observation frequency ν_s in GHz; (6) reference for the VLBI data; (7) 1 keV X-ray flux density F_X in μJy ; (8) reference for the X-ray flux. The X-ray flux densities are mainly chosen from Ghisellini (1993). For those sources which have multi-frequency VLBI observations, the VLBI data at the highest frequency are chosen.

3. Results

3.1. The derivation of the Doppler factor

By comparing the predicted and observed self-Compton flux, one can derive δ in the case of a moving sphere ($p=3+\alpha$) (Ghisellini et al. 1993)

$$\delta = f(\alpha) F_c \left[\frac{\ln(\nu_b/\nu_m)}{F_x \theta_d^{6+4\alpha} \nu_x^\alpha \nu_c^{5+3\alpha}} \right]^{1/(4+2\alpha)} \quad (3)$$

where F_m and F_x are the radio flux density and X-ray flux density in Jy, ν_x is in keV, ν_c is the frequency of VLBI observation in GHz, θ_d is in mas, ν_b is the synchrotron high frequency cutoff (assumed to be 10^{14} Hz), and the function $f(\alpha) = 0.08\alpha + 0.14$ (here $\alpha = 0.75$ is assumed). Recently, an improved approach was proposed by Jiang et al. (1998) to derive the Doppler factors based on an inhomogeneous jet model. However, the proper motion of knots is required in their derivation, which limits the number of sources in the sample. To make the sample as large as possible for the statistical analysis, we use the spherical model in this paper. The derived Doppler factors δ are listed in Table 2.

3.2. Correlation between ρ_{opt} and δ , ρ_{NIR} and δ

Also for the γ -ray flux densities of the EGRET sources, the maximum observed fluxes (> 100 MeV) are chosen. The γ -ray photon flux of is transferred into an integrated energy flux between 0.1 GeV and 5 GeV (i.e. $\nu_\gamma F_\gamma$). The reasons for choosing the maximum fluxes are: (1) all AGNs are variable sources and their radio emissions are mainly produced via synchrotron emission; (2) in the optical band, both the blue bump and the starlight account for part of the optical emission, the synchrotron radiation varies rapidly and the contribution of both the blue bump and the starlight can be reduced by using the maximum flux; (3) also, for the emission in the near infrared band, the contribution of thermal emission coming from the torus can be reduced. Figs. 1 and 2 show the ratio of the γ -ray flux to the optical flux versus the Doppler factor, and the ratio of the γ -ray flux to the infrared flux versus the Doppler factor, respectively. There is an obvious correlation between the flux density ratio and the Doppler factor. The relation between the flux ratio and the Doppler factor is:

$$\frac{(\nu F_\nu)_\gamma}{(\nu F_\nu)_{opt}} \propto \delta^{1.33}, \quad (4)$$

and

$$\frac{(\nu F_\nu)_\gamma}{(\nu F_\nu)_{NIR}} \propto \delta^{1.34}. \quad (5)$$

When BL Lac objects are excluded, the correlation remains present, but is less significant.

3.3. Correlation between ρ_{mm} and δ

Figs. 3 and 4 show the ratio of the γ -ray flux density to the millimeter (90 GHz, 230 GHz) flux density versus the Doppler factor. The correlation between ρ_{mm} and δ is poor. They improve when BL Lac objects are excluded, but are still poor in comparison to the optical and near-infrared cases.

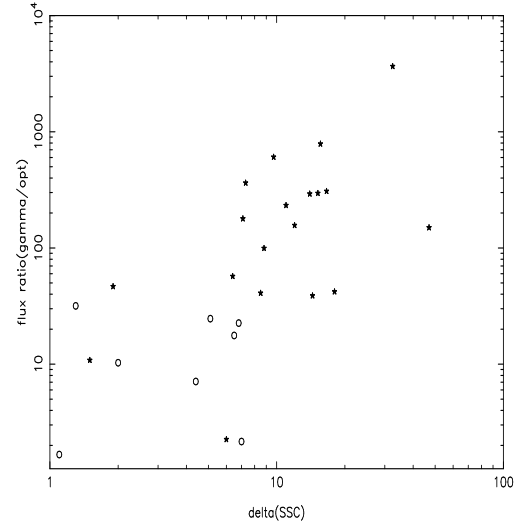


FIG 1

Fig. 1. Ratio of γ -ray flux to optical flux vs. Doppler factor δ . Circles: BL Lacs; Stars: quasars.

4. Discussion

That the soft photons are Compton up scattered to the γ -ray range by nonthermal electrons in the relativistically moving blobs might be the most favorable model for the γ -ray emission. The soft photons could come from synchrotron emission in the blob, namely the SSC process, or from outside the moving blob. Dermer (1995) proposed that the observed optically thin synchrotron flux density, combined with the Compton-scattered photon flux density, can be used to test whether the high-energy radiation is produced through SSC or external Compton scattering. We have examined the correlations between the ratio of the γ -ray flux density to the flux density in different wavebands and the Doppler factor δ . Two significant correlations are found, namely between ρ_{opt} and δ , and between ρ_{NIR} and δ , which support the external Compton scattering models for the high-energy γ -ray emission. The obtained correlations suggest that the observed flux densities in the optical and near-infrared wavebands are mainly due to optically thin synchrotron emission in the blobs. The relation between the emission in the optical band

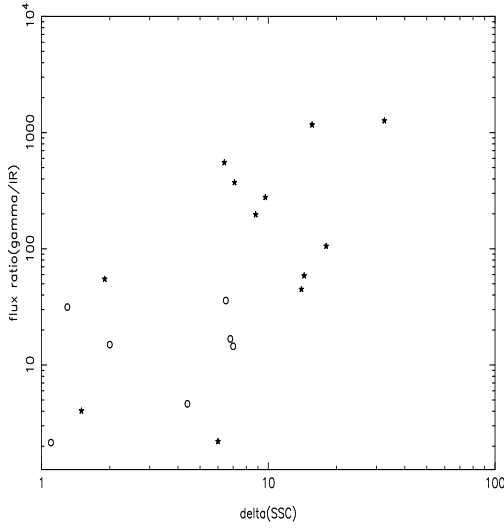


FIG 2

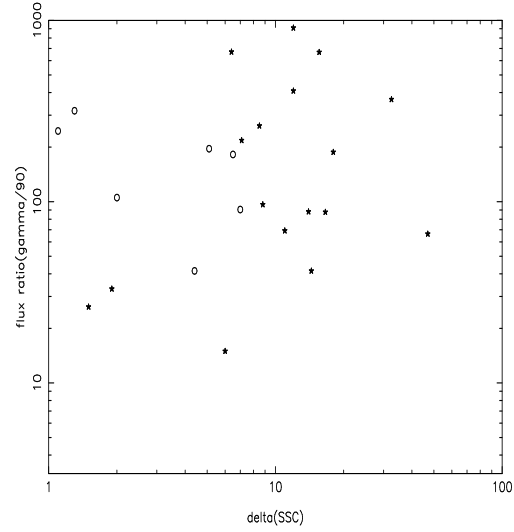


FIG 4

Fig. 2. Same as Fig. 1, but for the ratio of γ -ray flux to near infrared flux

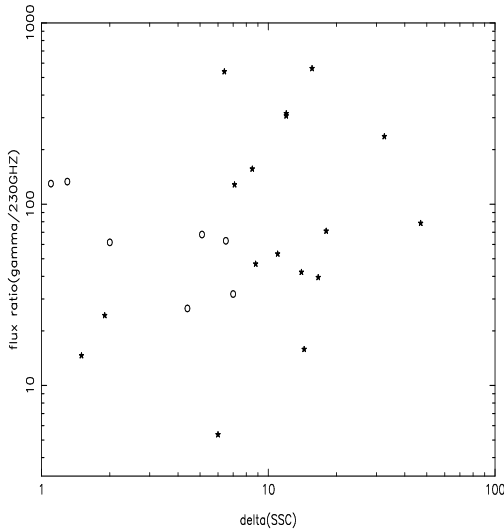


FIG 3

Fig. 3. Same as Fig. 1, but for the ratio of γ -ray flux to the flux at 230 GHz

and the emission in the γ -ray band was also shown by the facts that the highest γ -ray flux densities were recorded during the most prominent flare in the optical range for PKS 0420-014 (Wagner et al. 1995a) and that a rapid flare peaked about 22 hours after the optical outburst for PKS 1406-076 (Wagner et al. 1995b).

Table 3 also lists the values of b , which corresponds to $1 + \alpha$ in formula (1). The values of b are indeed close to $1 + \alpha$ ($\alpha = 0.75$ has been assumed), in the optical case and

Fig. 4. Same as Fig. 1, but for the ratio of γ -ray flux to the flux at 90 GHz

in the infrared case ($b = 1.33$ and $b = 1.34$, respectively). The k in formula (1) is the ratio of the isotropic energy density to the energy density of magnetic field, which is about 4-5 in the optical and NIR cases.

The Doppler factors δ of the BL Lac objects derived here are lower than those of other sources in the sample. The mechanism for X-ray radiation of BL Lac objects is still not quite clear. We used here a single model to derive the Doppler factor δ for all sources in the sample, including BL Lacs, on the assumption that SSC accounts for X-ray emission. However, some authors (Urry 1994) suggested that the X-ray emission from BL Lacs is due to synchrotron radiation instead of the synchrotron self-Compton radiation. If this is true, the derivation of the BL Lacs' Doppler factor δ here is questionable.

Compared with the optical and NIR cases, the correlation $\rho_{mm} - \delta$ is quite poor. One possible reason is that the synchrotron radiations in the millimeter wavebands is optically thick for some sources in the sample, whereas the theoretical model requires an optically thin synchrotron flux density. In addition, the correlations between the flux ratios and the Doppler factor show some deviation from the theoretical value $b = 1 + \alpha$. This may not be surprising since there are several factors that can affect the flux ratio ρ . For example, the SSC radiation may account for part of the γ -ray emission as well. For a few sources such as Mrk421, strong radiation is seen at TeV energies, and for others such as 3C273, the γ -ray emission is probably concentrated in MeV band, which will introduce errors in the correlation as well. In addition, the Doppler factor δ we have derived is based on the blob model. To obtain this result, one must know the core angular size and the flux

density at the turnover frequency. In practice, it is difficult to obtain this information, so one has to assume the VLBI observing frequency to be the synchrotron self-absorption frequency. Furthermore, a single $\alpha = 0.75$ is assumed for all sources in our sample. The derivation of the Doppler factor based on the blob model is clearly simplified.

By assuming that X-rays and γ -rays are cospacial, and deriving the size of the source using the variability time-scale, Dondi & Ghisellini (1993) derived a lower limit δ_γ on the Doppler factor of a source. They compared the Doppler factor with the flux ratio between the γ -ray flux density and the optical flux density and found a marginal correlation. They also listed the Doppler factors derived from the SSC model, but they did not compare the flux ratio with the δ_{SSC} . We compare their flux ratio with their δ_{SSC} and also find a strong correlation when excluding sources which were not identified with high confidence by Mattox et al (1997).

The strong correlations between $(\nu F_\nu)_\gamma / (\nu F_\nu)_{opt}$ and δ as well as $(\nu F_\nu)_\gamma / (\nu F_\nu)_{IR}$ and δ show that the γ -ray emission is more related to emission in the NIR-OPT band than to emission in the millimeter band. These results suggest that the relativistic electrons which are responsible for the optical emission are responsible for the γ -ray emission as well. This favors a model in which the γ -ray emission is due to inverse-Compton scattering on photons external to the jet.

5. Conclusion

We have studied a sample of EGRET AGNs which have recently been identified with high confidence and derive the Doppler factors for most of these gamma sources by using VLBI and X-ray data on the assumption of a homogeneous spherical emission plasma. Strong correlations between the flux ratio $\frac{(\nu F_\nu)_\gamma}{(\nu F_\nu)_{opt}}$ and δ as well as $\frac{(\nu F_\nu)_\gamma}{(\nu F_\nu)_{IR}}$ and δ are found, which is expected for inverse-Compton scattering on photons from outside the jet. The poor correlations between the flux ratio $\frac{(\nu F_\nu)_\gamma}{(\nu F_\nu)_{mm}}$ and δ may be due to the optically thick synchrotron emission in the millimeter wavelength for some EGRET sources.

Acknowledgements. We thank the referee, H. Bloemen, for his helpful comments and the linguistic improvements on the manuscript. The support from Pandeng Plan and NNSFC (No. 19703002) is gratefully acknowledged.

References

Baath L.B., Zhang F.J., & Chu H.S., 1991, A&A 250, 50
 Barthel P.D., Conway J.E., Myers S.T., Pearson T.J., & Readhead A.C.S., 1995, ApJ 444, L21
 Bloom S.D., Marscher A.P., Gear W.K., et al., 1994, AJ 108, 398
 Brown L.M.J., Robson E.I., Gear W.K., et al., 1989a, ApJ 340, 129
 Brown L.M.J., Robson E.I., Gear W.K., Smith M.G., 1989b, ApJ 340, 150
 Cawthorne T.V., Gabuzda D.C., 1996, MNRAS 278, 861
 Comastri A., Fossati G., Ghisellini G., Molendi S., 1997, ApJ 480, 534
 Dermer C.D., 1995, ApJ 446, L63
 Dermer C.D., Schlickeiser R., 1993, ApJ 416, 484
 Dermer C.D., Schlickeiser R., & Mastichiadis A., 1992, A&A 250, L27
 Dermer C.D., Sturner S.J., Schlickeiser R., 1997, ApJS 109, 103
 Dondi L., Ghisellini G., 1995, MNRAS 273, 583
 Falomo R., Dersanelli M., Bouchet P., Tanzi E.G., 1993, AJ 106, 11
 Fey A.L., Clegg A.W., Fomalont E.B., 1996, ApJS 105, 299
 Fichtel C.E., Bertsch D.L., Chiang J., et al., 1994, ApJS 94, 551
 Gabuzda D.C., Cawthorne T.V., Roberts D.H., & Wardle J.F.C., 1992, ApJ 388, 40
 Gabuzda D.C., Mullan C.M., Cawthorne T.V., et al., 1994, ApJ 435, 140
 Gear W.K., Robson E.I., Ade P.A.R., et al., 1985, ApJ 291, 511
 Gear W.K., Stevens J.A., Hughes D.H., et al., 1994, MNRAS 267, 167
 Ghisellini G., 1993, Adv.Space Res., Vol.13, No, 12, 587
 Ghisellini G., Maraschi L., 1989, ApJ 340, 181
 Ghisellini G., Padovani P., Celotti A., Maraschi L., 1993, ApJ 407, 65
 Impey C.D., Neugebauer G., 1988, AJ 95, 307
 Jiang D.R., Cao X., Hong X., 1998, ApJ 494, 139
 Jones T.W., O'Dell S.L., Stein W.A., 1974, ApJ 188, 353
 Königl A., 1981, ApJ 243, 700
 Kellerman K.I., Shaffer D.B., Purcell G.H., et al., 1977, ApJ 211, 658
 Landau R., Golisch B., Jones T.J., et al., 1986, ApJ 308, 78
 Mannheim K., 1993a, A&A 269, 67
 Mannheim K., 1993b, Phys.Rev.D 48, 2408
 Mannheim K., Biermann P.L., 1992, A&A 53, L21
 Maraschi L., Ghisellini G., Celotti A., 1992, ApJ 397, L5
 Marscher A.P., 1980, ApJ 235, 386
 Marscher A.P., Gear W.K., 1985, ApJ 298, 114
 Mastichiadis A., Protheroe R.J., 1990, MNRAS 246, 279
 Mattox J.R., Schachter J., Molnar L., et al., 1997, ApJ 481, 95
 Mead A.R.G., Ballard K.R., Brand P.W.J.L., et al., 1990, A&AS 83, 183
 Melia F., Königl A., 1989, ApJ 340, 162
 Pearson T.J., Readhead A.C.S., 1988, ApJ 328, 114
 Pohl M., Reich W., Krichbaum T.P., et al., 1995, A&A 303, 383
 Rieke G.H., Lebofsky M.J., Wisniewski W.Z., 1982, ApJ 263, 73
 Sambruna R.M., Maraschi L., Urry C.M., 1996, ApJ 463, 444
 Shen Z.Q., Wan T.S., Moran J.M., et al., 1997, AJ 114, 1999
 Shen Z.Q., Wan T.S., Moran J.M., et al., 1998, AJ 115, 1357
 Sikora M., Begelman M.C., Rees M.J., 1994, ApJ 421, 153
 Steppe H., Salter C.J., Chini R., et al., 1988, A&AS 75, 317
 Steppe H., Leichti S., Mauersberger R., et al., 1992, A&AS 96, 441
 Steppe H., Jeyakumar S., Saikia D.J., Salter C.J., 1995, A&AS 113, 409
 Thompson D.J., Bertsch D.L., Dingus B.L., et al., 1995, ApJS 101, 259

Urry C.M., 1994, in *Frontiers of Space and Ground-base Astronomy*, ed. Wamsteker W., Longair M.S., Kondo Y.(Netherlands:Kluwer), 335

Vermeulen R.C., Cohen M.H., 1994, *ApJ* 430, 467

Von Montigny C., Bertsch D.L., Dingus B.L., et al., 1996, *A&AS* 120, 519

Wagner S.J., Camenzind M., Dreissigacker O., et al., 1995a, *A&A* 298, 688

Wagner S.J., Mattox J.R., Hopp U., Beck H., et al., 1995b, *ApJ* 454, L97

Wehrle A.E., Unwin S.C., Zook A.C., et al., 1996, In *Blazar Continuum Variability*, ASP Conf.Ser. 110:430-35. San Francisco: Astron.Soc.Pac

Worrall D.M., Wilkes B.J., 1990, *ApJ* 360, 396

Xu W., Readhead A.C.S., Pearson T. J., 1995, *ApJS* 99, 297

Zhang Y.F., Marscher A.P., Aller H.D., et al., 1994, *ApJ* 432, 91

Table 1. Basic parameters of the selected AGNs (see text for details)

IAU NAME	class	redshift	F_{γ}	α_{γ}	Ref.	F_{opt} mJy	Ref.	F_{IR} mJy	Ref.	F_{90} Jy	Ref.	F_{230} Jy	Ref.
0208-512	HPQ	1.003	110.	0.7	(14)	0.66	(6)						
0234+285	HPQ	1.213	66.3	1.7	(15)	0.156	(6)		3.08	(4)	2.66	(4)	
0235+164	B	0.94	82.5	0.9	(15)	6.6	(6)	11.8	(11)	3.6	(3)	4.06	(4)
0336-019	HPQ	0.852	400	1.4	(17)	0.45	(7)	(1.1)	(11)	2.98	(4)	1.38	(4)
0420-014	HPQ	0.915	61.2	0.9	(15)	0.296	(6)	7.0	(10)	5.52	(3)	4.49	(4)
0458-020	HPQ	2.286	31.	1.5	(17)	0.17	(6)			2.16	(4)	0.71	(3)
0521-365	HPQ	0.0554	20.7	1.2	(15)	2.0	(6)	19.5	(12)	4.63	(3)	3.24	(4)
0528+134	LPQ	2.06	295.	1.6	(15)	0.062	(6)	0.65	(18)	3.48	(1)	2.1	(1)
0537-441	B	0.894	36.4	1.0	(15)	2.05	(6)	10.0	(12)				
0716+714	B	0.3	50	1.4	(14)	20.5	(6)	11.1	(9)	2.75	(3)	3.03	(4)
0735+178	B	0.424	86.3	1.5	(15)	6.9	(6)	17.2	(13)	3.79	(4)	2.52	(4)
0836+710	LPQ	2.172	45.3	1.4	(15)	0.98	(6)			0.86	(2)	0.56	(2)
0954+658	B	0.368	14.3	0.9	(15)	0.82	(7)			0.58	(2)	0.65	(2)
1101+384	B	0.031	21.	0.9	(14)	17.8	(6)	50.1	(11)	0.68	(1)	0.5	(1)
1127-145	NP	1.187	93.2	1.15	(17)	0.652	(8)			0.63	(5)	0.73	(5)
1156+295	HPQ	0.729	229.	1.0	(17)	5.1	(6)	1.91	(13)	2.44	(4)	1.18	(3)
1219+285	B	0.102	32.2	0.3	(16)	2.9	(7)	10.6	(13)	1.63	(2)	1.51	(2)
1226+023	LPQ	0.158	62.6	1.4	(16)	24.6	(6)	91.4	(13)	20.8	(3)	22.6	(4)
1253-055	HPQ	0.538	450	0.9	(17)	15.1	(6)	21.9	(11)	19.1	(4)	19.6	(4)
1510-089	HPQ	0.361	56.2	1.51	(15)	1.18	(6)	2.83	(11)	6.22	(3)	6.34	(3)
1611+343	LPQ	1.40	54.9	1.0	(15)	0.39	(6)	0.68	(1)	1.8	(1)	1.19	(1)
1633+382	LPQ	1.814	105.4	0.9	(15)	0.246	(6)	1.95	(1)	2.05	(1)	1.03	(1)
1730-130	LPQ	0.902	136.9	1.4	(15)	0.52	(8)			9.85	(4)	4.98	(3)
1739+522	HPQ	1.375	53.8	1.2	(15)	0.155	(6)						
2200+420	B	0.069	40	1.2	(17)	5.9	(7)	32.76	(11)	5.67	(4)	3.44	(4)
2230+114	HPQ	1.037	28.5	1.6	(15)	0.47	(6)	1.45	(11)	3.73	(4)	1.97	(4)
2251+158	HPQ	0.859	135	1.2	(14)	1.42	(6)	2.6	(10)	8.23	(4)	6.6	(3)

- (1) Bloom et al., 1994
- (2) Gear et al., 1994
- (3) Steppe et al., 1988
- (4) Steppe et al., 1992
- (5) Steppe et al., 1995
- (6) Dondi & Ghisellini, 1995
- (7) Ghisellini et al., 1993
- (8) Comastri et al., 1996
- (9) Sambruna et al., 1996
- (10) Gear et al., 1985
- (11) Mead et al., 1990
- (12) Falomo et al., 1993
- (13) Landau et al., 1986
- (14) Fichtel et al., 1994
- (15) Thompson et al., 1995
- (16) Von Montigny et al., 1996
- (17) Mattox et al., 1997
- (18) Rieke et al., 1982

Table 2. VLBI and X-ray data of the selected AGNs

Source	z	θ_d mas	$S_c(\nu_s)$ Jy	ν_s GHz	Ref.	S_X μ Jy	Ref.	derived δ
0208-512	1.003	0.35	2.77	5.0	(4)	0.61	(15)	15.2
0234+285	1.213	0.09	1.7	22.3	(5)	0.15	(5)	16.6
0235+164	0.94	0.5	1.75	5.0	(5)	0.17	(5)	6.5
0336-019	0.852	0.57	1.52	2.3	(5)	0.047	(5)	15.6
0420-014	0.915	0.17	1.6	8.4	(16)	0.52	(5)	14.0
0458-020	2.286	0.28	2.62	5.0	(2)	0.1	(3)	47.0
0521-365	0.0554	0.73	1.82	5.0	(4)	0.68	(5)	1.5
0528+134	2.06	0.08	3.0	22	(8)	1.59	(10)	32.5
0537-441	0.894	0.6	3.37	5	(4)	0.81	(15)	6.8
0716+714	> 0.3	0.16	0.631	5.0	(6)	1.28	(15)	7.0
0735+178	0.424	0.24	1.85	22.2	(9)	0.32	(5)	2.0
0836+710	2.172	0.34	1.05	5.0	(11)	1.6	(15)	8.0
0954+658	0.368	0.19	0.48	5.0	(12)	0.5	(5)	5.1
1101+384	0.031	0.24	0.366	5.0	(6)	14.0	(5)	1.1
1127-145	1.187	0.95	3.27	2.3	(1)	0.34	(15)	12.0
1156+295	0.729	0.123	1.4	22.2	(5)	0.15	(5)	6.4
1219+285	0.102	0.20	0.159	5.0	(13)	0.42	(5)	1.3
1226+023	0.158	0.14	3.49	15.	(5)	21	(5)	6.0
1253-055	0.538	0.14	4.84	15.	(5)	1.4	(5)	18.
1510-089	0.361	0.12	2.76	15	(5)	0.44	(5)	14.4
1611+343	1.40	< 0.38	2.14	8.55	(1)	0.24	(15)	7.1
1633+382	1.814	0.5	5.4	10.7	(14)	0.08	(3)	12.0
1730-130	0.902	0.42	2.34	5	(2)	0.2	(5)	11
1739+522	1.375	0.37	0.89	5.0	(5)	0.1	(5)	7.3
2200+420	0.069	0.35	1.6	5.0	(5)	0.82	(5)	4.4
2230+114	1.037	0.50	0.54	5.0	(5)	0.34	(5)	1.9
2251+158	0.859	0.54	5.226	5.0	(7)	5.5	(3)	8.8

- (1) Fey et al., 1996
- (2) Shen et al., 1997
- (3) Dondi & Ghisellini, 1995
- (4) Shen et al., 1998
- (5) Ghisellini et al., 1993
- (6) Xu et al, 1995
- (7) Cawthorne & Gabuzda, 1996
- (8) Pohl et al., 1995
- (9) Baath et al., 1991
- (10) Zhang et al., 1994
- (11) Pearson & Readhead, 1988
- (12) Gabuzda et al., 1992
- (13) Gabuzda et al., 1994
- (14) Kellerman et al., 1977
- (15) Comastri et al., 1997
- (16) Wagner et al., 1995a

Table 3. Results of the linear regression analysis

y	x	N	a	b	r	P	note.
$\log \frac{(\nu F_\nu)_\gamma}{(\nu F_\nu)_{opt}}$	$\log(\delta)$	27	0.61	1.33	0.66	2×10^{-4}	excluding BL Lac objects
		19	0.94	1.15	0.57	1.05×10^{-2}	
$\log \frac{(\nu F_\nu)_\gamma}{(\nu F_\nu)_{NIR}}$	$\log(\delta)$	19	0.64	1.34	0.65	2.5×10^{-3}	excluding BL Lac objects
		12	0.8	1.32	0.59	4.5×10^{-2}	
$\log \frac{(\nu F_\nu)_\gamma}{(\nu F_\nu)_{230GHz}}$	$\log(\delta)$	24	1.6	0.26	0.22	0.3	excluding BL Lac objects
		17	1.3	0.58	0.14	0.14	
$\log \frac{(\nu F_\nu)_\gamma}{(\nu F_\nu)_{90GHz}}$	$\log(\delta)$	24	2.0	0.19	0.12	0.4	excluding BL LAC objects
		17	1.59	0.53	0.37	0.14	

Notes: The linear regression is obtained by considering x to be the independent variable and assuming a relation $y=a+bx$; N is the number of points, r is the correlation coefficient, and P is the chance probability.